X-ray magnetic circular dichroism in GdN: First-principles calculations

V. N. Antonov,[1,2,3] B. N. Harmon,[1] A. N. Yaresko,[2] and A. P. Shpak[3]
[1]*Ames Laboratory, Iowa State University, Iowa 50011, USA*
[2]*Max Planck Institute for the Physics of Complex Systems, D-01187 Dresden, Germany*
[3]*Institute of Metal Physics, 36 Vernadsky Street, 03142 Kiev, Ukraine*
(Received 13 December 2006; revised manuscript received 13 April 2007; published 18 May 2007)

GdN is a system with a strongly correlated electronic structure and a low concentration of free charge carriers. The x-ray magnetic circular dichroism (XMCD) spectra of GdN at the Gd $L_{2,3}$, $M_{4,5}$ and N K edges are investigated theoretically from first principles, using the fully relativistic Dirac linear muffin-tin orbital band structure method. The electronic structure is obtained with the local spin-density approximation (LSDA), as well as the LSDA+U method. The origin of the XMCD spectra in the compound is examined. The core-hole effect in the final states has been investigated using a supercell approximation. The final-state interaction improves the agreement between the theory and the experiment at the Gd $M_{4,5}$ and N K edges, however, it has a minor influence on the shape of the Gd $L_{2,3}$ XMCD spectra. We found also a strong influence of the surface on the x-ray absorption spectrum at the N K edge.

DOI: 10.1103/PhysRevB.75.184422 PACS number(s): 75.30.Mb, 71.28.+d

I. INTRODUCTION

The Gd pnictides form an interesting family of materials, because of the great variety of their magnetic and electrical properties, despite their common simple crystal structure, the face-centered cubic of sodium chloride. While most Gd pnictides have been found to be antiferromagnetic, stoichiometric GdN after a controversial discussion over three decades[1,2] seems to be recognized now as a ferromagnet. It has a Curie temperature T_C around 60 K and a magnetic saturation moment near $7\mu_B$/Gd ion consistent with the $^8S_{7/2}$ half filled $4f$ shell configuration of Gd^{3+} with zero orbital angular momentum.[3]

An appealing property of GdN is that it is ferromagnetic with a large gap at the Fermi energy in the minority spin states, according to the electronic structure calculations based on the local density approximation.[4–6] At the same time, GdN is semimetallic in majority spin states with electron and hole pockets at the Fermi surface.[5] This latter property has led to some interest in GdN as a possible candidate for spin-dependent transport devices,[7] exploiting the spin filter, giant magnetoresistance, or tunneling magnetoresistance effects.

The first band-structure investigation of the Gd monopnictides (GdSb, GdAs, GdP, and GdN) was carried out by Hasegawa and Yanase in Ref. 4 using the augmented plane wave method. Later Petukhov *et al.*[5] presented the results of first-principles calculations of the electronic band structures, equilibrium lattice constants, cohesive energies, bulk moduli, and magnetic moments for the rare-earth pnictides including GdN using the linear-muffin-tin-orbital method. The $4f$ states were treated as localized corelike states with fixed spin occupancies. They estimated quasiparticle self-energy corrections using an approach previously used for semiconductors. With these corrections, GdN is found to be a semiconductor in the paramagnetic phase and a semimetal in the ferromagnetic phase.

It is well known that the LSDA fails to describe the electronic structure and properties of $4f$ electron systems in which the interaction among the electrons are strong.[8] In recent years more advanced methods of electronic structure determination such as LSDA plus self-interaction corrections (SIC–LSDA),[9] the LSDA+U (Ref. 10) method, the GW approximation[11] and dynamical mean-field theory (DMFT)[12–14] have sought to remedy this problem and have met with considerable success.

The band structure and the optical response functions of GdN were investigated by Lambrecht[6] using the linear muffin-tin orbital (LMTO) method taking into account quasiparticle corrections using simplified GW approximation. He concluded that GdN is an indirect narrow gap semiconductor. Aerts *et al.*[15] predicted, on the basis of the SIC-LSDA electronic structure calculation, an indirect band gap of 0.9 eV for the minority spin channel only, and a principal Gd s,d and N p-like symmetry of the majority electrons at the Fermi energy. The ordered magnetism of GdN originates from the large local spin magnetic moments of the half filled Gd $4f$ shell coupled by indirect exchange interactions. Duan *et al.*[16] investigated the electronic structure and magnetic properties of GdN as a function of unit cell volume using the LSDA+U method. They observed a transformation in the conduction properties associated with the volume increase: first from half-metallic to semimetallic, then ultimately to semiconducting. Applying stress can alter the carrier concentration as well as mobility of the holes and electrons in the majority spin channel. They found that the exchange parameters depend strongly on lattice constant, thus the Curie temperature of this system can be enhanced by applying stress or by doping impurities. Kalvoda *et al.*[17] apply *ab initio* quantum-chemical methods to calculate correlation effects on cohesive properties of GdN. The calculated values of cohesive energy and lattice constant were found to be in reasonable agreement with the experimental data. Those authors also estimated a bulk modulus. Taking into account estimates for the effect of a better basis both at the one-particle level and at the many-particle level, they reach 98.5% of the experimental cohesive energy and 101.3% of the experimental lattice constant. Sharma and Nolting[18] investigated the temperature dependent electronic correlation effects in the con-

duction Gd 5*d* bands of GdN based on the combination of many-body analysis of the multiband Kondo lattice model and first principles TB-LMTO band-structure calculations. Physical properties such as the quasiparticle density of states, spectral density, and quasiparticle band structure were calculated and discussed. A redshift of 0.34 eV of the lower band edge was obtained and found to be in close agreement with earlier theoretical predictions and experimental values. The electronic structure calculation of Gd monopnictides including GdN has been performed by Ghosh *et al.* using the LMTO method in the LSDA+U approximation.[19] They also calculated optical and magneto-optical properties such as the optical reflectivity, the dielectric function and the complex Kerr effect. Reflectivity calculations reveal a plasma edge effect in GdP, GdAs, and GdSb and agree well with the experimental results. They found that the deep plasma minimum results in a large Kerr rotation in GdP, GdAs, and GdSb. A study of the electronic structure and magnetic properties of Gd pnictides was reported also by Larson and Lambrecht.[20] The calculations were performed using a full-potential LMTO method within the LSDA+U approach. They used Hubbard $U=8$ and 3.4 eV for Gd 4*f* and 5*d* states, respectively. From calculations with different magnetic configurations, a Heisenberg model with first and second nearest-neighbor exchange parameters was extracted. The Heisenberg model was then used to predict Curie-Weiss and Neel temperatures and critical magnetic fields within mean field approximation. The trends were found to be in good agreement with the experimental data.

In the present study, we focus our attention on the theoretical investigation of the x-ray magnetic circular dichroism in GdN. The XMCD technique developed in recent years has evolved into a powerful magnetometry tool to separate orbital and spin contributions to element specific magnetic moments. XMCD experiments measure the difference in absorption of x rays with opposite (left and right) states of circular polarization.

X-ray absorption spectra (XAS) and XMCD at the gadolinium $M_{4,5}$ and N K edges have been measured in GdN by Leuenberger *et al.*[21] The ordered 4*f* moment extracted from the $M_{4,5}$ XMCD spectra was consistent with the $^8S_{7/2}$ configuration of Gd^{3+}. The exchange field generated by the Gd 4*f* electrons in the ferromagnetic phase of GdN induces a magnetic polarization of the N *p* band states, as can be concluded from the observation of strong magnetic circular dichroism at the *K* edge of nitrogen. However, a comparison of the spectra with the theoretical partial density of vacant N *p* states shows considerable disparities that are not well understood.

Leuenberger *et al.*[22] measured core-level x-ray-absorption spectra and x-ray magnetic circular dichroism at the Gd $L_{2,3}$ edges in thin films of the GdN with a unit-cell volume 8.6% above that of bulklike layers. The Curie temperature T_C, a key quantity for magnetism, amounts to only half the bulk value of 60 K indicating a significant reduction of the effective exchange interaction between the 4*f* states. An intriguing observation is that the ratio of the dichroic signal amplitudes in the lattice-expanded layers, L_3/L_2, is up to three times higher than the value expected and observed for the bulklike layers. This is mainly due to a reduced L_2 XMCD amplitude.

Leuenberger *et al.*[23] also measured the XA and XMCD spectra in artificial nanoscale ferrimagnetic multilayers GdN/Fe at Gd $M_{4,5}$, $L_{2,3}$ and Fe K and $L_{2,3}$ edges to separate the contributions of the component layers to the magnetization and local magnetic structure.

This paper is organized as follows. Section II presents a description of the GdN crystal structure as well as the computational details. Section III is devoted to the electronic structure and XMCD spectra of the GdN calculated with the fully relativistic Dirac LMTO band structure method. The calculated results are compared with the available experimental data. Finally, the results are summarized in Sec. IV.

II. CRYSTAL STRUCTURE AND COMPUTATIONAL DETAILS

The details of the computational method are described in our previous papers,[8,24] and here we only mention several aspects. The calculations have been performed for the face-centered cubic structure of sodium chloride (space group $Fm\bar{3}m$, No. 225) with lattice constant $a=4.92$ Å using the spin-polarized linear-muffin-tin-orbital (LMTO) method[25,26] with the combined correction term taken into account. We used the Perdew-Wang[27] parametrization for the exchange-correlation potential. Brillouin zone (BZ) integrations were performed using the improved tetrahedron method[28] and charge self-consistently was obtained with 349 irreducible **k** points. To improve the potential we include additional empty spheres. The basis consisted of Gd *s*, *p*, *d*, and *f*; N *s*, *p*, and *d*; and empty spheres *s*, and *p* LMTO's.

The intrinsic broadening mechanisms have been accounted for by folding XMCD spectra with a Lorentzian. For the finite lifetime of the core hole a constant width Γ_c, in general form,[29] has been used. The finite apparative resolution of the spectrometer has been accounted for by a Gaussian of 0.6 eV.

In order to simplify the comparison of the theoretical x-ray isotropic absorption spectra of GdN to the experimental ones we take into account the background intensity which affects the high energy part of the spectra and is caused by different kinds of inelastic scattering of the electron promoted to the conduction band above the Fermi level due to x-ray absorption (scattering on potentials of surrounding atoms, defects, phonons, etc.). To calculate the background spectra we used the model proposed by Richtmyer *et al.*[30] (for details see Ref. 31).

We have adopted the LSDA+U method[10] as a different level of approximation to treat the electron-electron correlations. We used the rotationally invariant LSDA+U method. This method is described in detail in our previous paper.[32] The effective on-site Coulomb repulsion U was considered as an adjustable parameter. We used $U=8$ eV, for this value we found good agreement between the energy position of the occupied Gd 4*f* DOS and corresponding peak in the x-ray photoemission (XPS) spectrum.[21] For the exchange integral J the value of 0.66 eV estimated from constrained LSDA calculations was used.

III. RESULTS AND DISCUSSION

A. Energy band structure

Figure 1 shows the fully relativistic spin-polarized energy band structure of GdN. In these calculations the 4*f* states

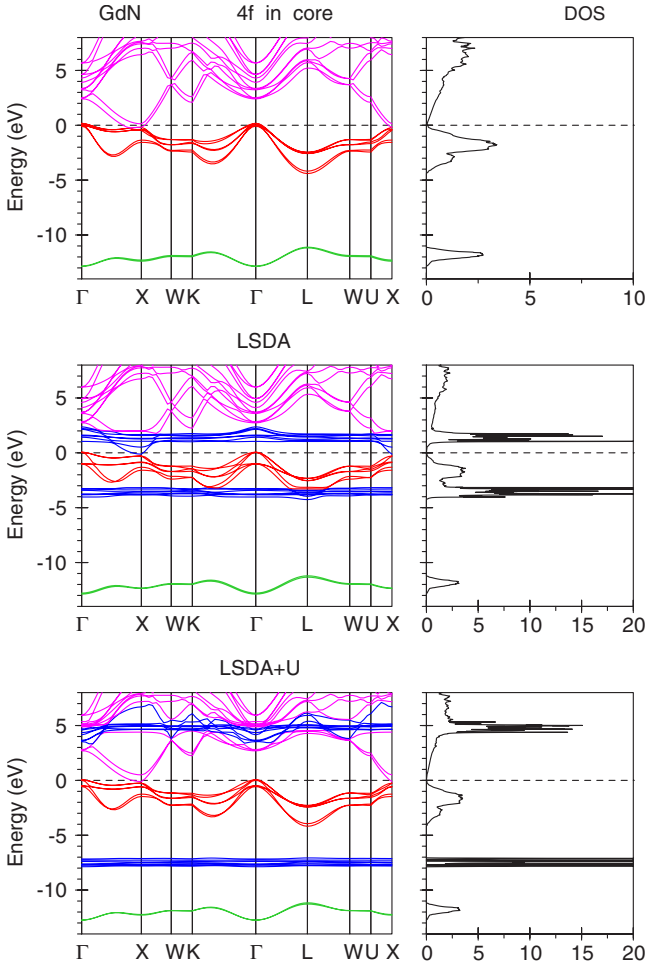

FIG. 1. (Color online) Self-consistent fully relativistic spin-polarized energy band structure and total DOS [in states/(unit cell eV)] calculated for GdN treating the 4*f* states as (1) fully localized (4*f* in core), (2) itinerant (LSDA), and (3) partly localized (LSDA +*U*).

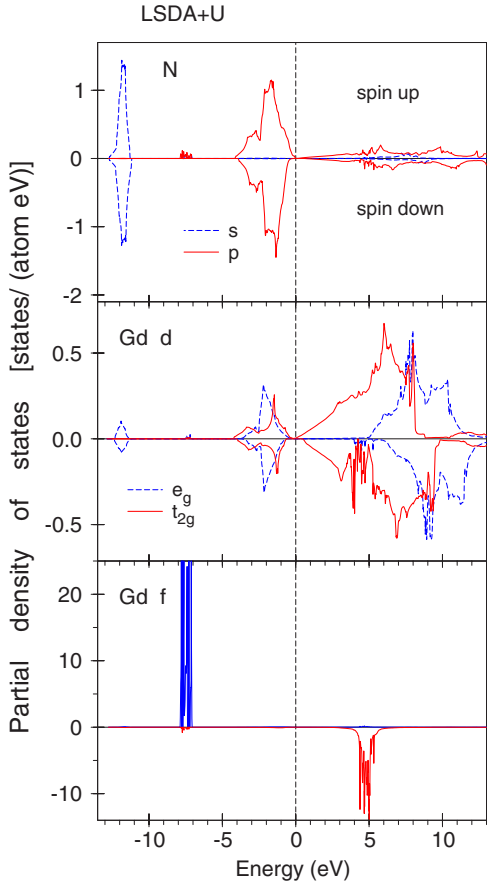

FIG. 2. (Color online) Partial density of states [in states/(atom eV)] of GdN. The Fermi energy is at zero.

have been considered as (1) itinerant using the local spin-density approximation, (2) fully localized, treating them as core states, and (3) partly localized using the LSDA+*U* approximation.

The energy band structure of GdN with the 4*f* electrons in core can be subdivided into three regions separated by energy gaps. The bands in the lowest region around −12.9 to −11.1 eV have mostly N *s* character with some amount of Gd *sp* character mixed in. The next six energy bands are primarily N *p* bands separated from the *s* bands by an energy gap of about 6.2 eV. The width of the N *p* band is about 4.5 eV and is influenced by hybridization with Gd 5*d* states. The spin splitting of the N *p* bands is small [about 0.2 eV at the *X* symmetry point (Fig. 1)]. The highest region can be characterized as Gd crystal field and spin-split *d* bands.

An important issue is the energy position of the occupied 4*f* states in the electron band structure of GdN. The LSDA calculations place the empty 4*f* states of Gd in GdN at 1 to 2 eV above the Fermi level with the occupied majority-spin 4*f* states situated at around −4 to −3.2 eV below Fermi level E_F. It is well known that LSDA usually gives a wrong energy position for the 4*f* states in rare-earth compounds. For non-zero 4*f* occupation it places the 4*f* states right at the Fermi level[33,34] in contradiction with various experimental observations. In the case of Gd compounds the LSDA places the empty 4*f* states too close to the Fermi energy. For example, the LSDA calculations produce the empty 4*f* states in pure Gd metal at 2.7 eV above the Fermi level,[35] although according to the x-ray bremsstrahlung isochromat spectroscopy (BIS) measurements they are situated around 5.5 eV above the Fermi level.[36,37] The XPS spectrum measured by Leuenberger *et al.*[21] in the valence band region of GdN shows the Gd^{3+} $4f^6$ final state multiplet located at around 8 eV below the Fermi level.

Figure 1 also presents the energy band structure of GdN calculated in the LSDA+*U* approximation. The results agree well with previous LSDA+*U* band structure calculations.[16,20] In such an approximation the Gd 4*f* empty states are situated around 5 eV above the Fermi level, well hybridized with Gd 5*d* and N 2*p* minority states. The majority-spin 4*f* states form a narrow band well below the Fermi energy and occupy a −7 to −8 eV energy interval in good agreement with the XPS measurements.[21]

The partial density of states (DOS) of cubic ferromagnetic GdN are presented in Fig. 2 for the LSDA+*U* calculations. The majority 4*f* electrons create an exchange field that leads to spin splitting of the N *p* band. Furthermore, there is a visible Gd *d* – N *sp* as well as Gd 4*f* – N *p* hybridization in

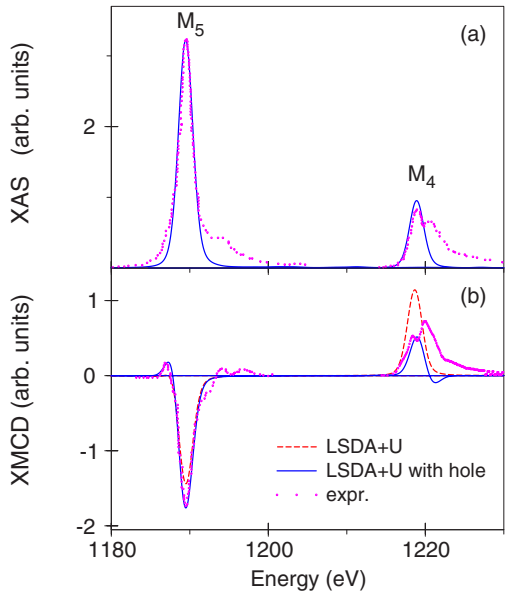

FIG. 3. (Color online) (a) Theoretically calculated (dotted lines) and experimental (Ref. 21) (circles) isotropic absorption spectra of GdN at the Gd $M_{4,5}$ edges. Experimental spectra were measured with external magnetic field (0.1 T) at 15 K; (b) experimental (Ref. 21) (circles) XMCD spectra of GdN at the Gd $M_{4,5}$ edges in comparison with theoretically calculated ones using the LSDA+U approximation without (dotted lines) and with (full lines) taking into account core-hole effect.

occupied part of GdN valence band. One of the consequences is that the N anion should carry a magnetic moment. The Gd f states above the Fermi level hybridize with the Gd $d_{t_{2g}}$ states only in the minority channel (Fig. 2). The Gd d_{e_g} states shift to higher energy due to the crystal-field splitting and almost do not hybridize with the Gd $4f$ states. The orbital moments are equal to $0.057\mu_B$ and $-0.0007\mu_B$ on the Gd and N sites, respectively. Exchange and hybridization induce spin splitting of the conduction band states. As a result, the itinerant Gd $5d$ and N $2p$ derived band electrons carry small spin magnetic moments of $0.107\mu_B$ and $-0.098\mu_B$, respectively that are of opposite each other and nearly cancel. The Gd $5d$ and N $2p$ orbital moments are equal to $-0.0066\mu_B$ and $-0.0007\mu_B$, respectively.

One should mentioned that although Gd^{3+} free ion consistent with the $^8S_{7/2}$ half filled $4f$ shell configuration possesses a zero orbital angular momentum, in solids Gd has small but nonzero orbital moment of around $0.063\mu_B$ due to hybridization with other states and also because in solids spin-up states are the linear combination of the $4f_{5/2}$ and $4f_{7/2}$ states and m_l for each state can be noninteger.

B. Gd $M_{4,5}$ XMCD spectra

The study of the $4f$ electron shell in rare earth compounds is usually performed by tuning the energy of the x-ray close to the $M_{4,5}$ edges of rare-earth where electronic transitions between $3d_{3/2,5/2}$ and $4f_{5/2,7/2}$ states are involved. Figure 3 shows the calculated XAS and XMCD spectra in the LSDA+U approximation for GdN at the $M_{4,5}$ edges together with the corresponding experimental data.[21] The experimentally measured dichroism is large, as is common for Gd-based systems at the $3d$ threshold; it amounts to more than 20%.

The theoretically calculated XAS spectra have a rather simple line shape composed of two white line peaks at the M_5 and M_4 edges, however, the experimentally measured spectra have well pronounced fine structures at high energy part of the M_5 and M_4 XAS's. We should mention here that a major shortcoming in band structure approximation is that the multiplet structure has not been included. For the N K and Gd $L_{2,3}$ edges this is probably not a major problem. However, for Gd $M_{4,5}$ edges the core-valence electrostatic interactions can significantly influence the line shape of the XAS and XMCD spectra. Thole *et al.*[38] measured and calculated in intermediate coupling the $M_{4,5}$ XAS for all the rare-earth metals. These authors found that the number of $3d^94f^{n+1}$ final-state levels reaches to 1077 in Gd^{3+}. The XAS features are situated in two groups whose separation corresponds roughly to the $3d_{3/2}-d_{5/2}$ spin-orbit splitting. Although the calculations indicate that the vast majority of lines have a small weight, nevertheless, this weight adds up to recognizable shoulders in the M_4 and M_5 spectra on the high energy side. Therefore the fine structure on the high energy side of Gd $M_{4,5}$ XAS's in GdN (Fig. 3) are believed to be due to the multiplet structures which have not been included in present calculations. A theoretical method which includes consistently both the band structure and atomiclike multiplet structure of rare earth metals and compounds is highly desired.

Figure 3(b) shows the calculated XMCD spectra in the LSDA+U approximation for GdN together with the corresponding experimental data.[21] The Dirac-Hartree-Fock-Slater one particle approximation used in this work to calculate the core states is not able to produce a correct energy position of the spectra (due to not taking into account a self-interaction correction, different kinds of relaxation processes and other many-particle effects), therefore we used the experimentally measured positions of the spectra. The dichroism is mostly negative at the Gd M_5 edge and positive at the M_4 one. The calculations describe correctly the deep negative minimum at the Gd M_5 edge and the low energy positive peak at the M_4 edge, however, they do not produce the high energy fine structures at both the edges, which are probably caused by the multiplet structure as described above. The XMCD at the M_5 edge also possesses an additional small positive lobe at the low energy side which is not in the theoretical calculations. The LSDA+U theory underestimates the intensity for the XMCD spectrum at M_5 edge and overestimates it at the M_4 edge in comparison with the experiment.

We investigate also the effect of the core-hole effect in the final state using the supercell approximation. A similar approximation has been used by several authors.[39,40] When the $3d$ core electron is photoexcited to the unoccupied $4f$ states, the distribution of the charge changes to account for the created hole. The final-state interaction improves the agreement between theory and the experiment at the M_5 edge in the intensity of the prominent negative peak and by producing correctly a positive lobe at the low energy side.

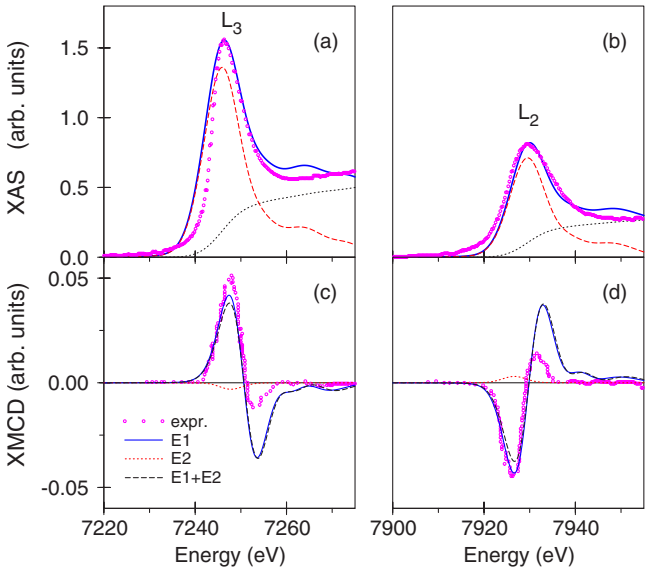

FIG. 4. (Color online) (a), (b) Theoretically calculated (dashed line) and experimental (Ref. 22) (circles) isotropic absorption spectra of GdN at the Gd L_3 and L_2 edges. Experimental spectra were measured at a bulklike GdN layer deposited on a Si substrate at 450 °C in total fluorescence yield mode. Dotted lines show the theoretically calculated background spectra, full thick lines are sum of the theoretical XAS and background spectra; (c), (d) experimental (Ref. 22) (circles) XMCD spectra of GdN at the Gd L_3 and L_2 edges in comparison with theoretically calculated ones in the LSDA+U approximation taking into account only dipole allowed E_1 transitions (full lines), only quadrupole $p \rightarrow f$, E_2 transitions (dotted lines) and sum of E_1 and E_2 transitions (dashed lines).

C. Gd $L_{2,3}$ XMCD spectra

Figure 4 shows the calculated XAS and XMCD spectra in the LSDA+U approximation at the $L_{2,3}$ edges together with the corresponding experimental data measured at bulklike layers of GdN.[22]

The dichroism at the $L_{2,3}$ edges has two lobes, a positive and a negative one. The positive lobe is larger in comparison with the negative one for L_3 spectrum and vice versa for the L_2 edge. Our LSDA+U calculations overestimate the smaller lobe and underestimate the larger one at both the L_3 and L_2 edges.

We found minor influence of the final-state interaction on the shape of the Gd $L_{2,3}$ XMCD spectra in the whole energy interval. A small core-hole effect might come from the fact that the Gd $5d$ states are less localized in comparison with the $4f$ states and have smaller amplitude inside the MT sphere and thus are less subject to the core hole potential.

We investigate also the effect of the electric quadrupole E_2 and magnetic dipole M_1 transitions. We found that the M_1 transitions are extremely small in comparison with the E_2 transitions and can be neglected. The E_2 transitions are much weaker than electric dipole transitions E_1 and almost invisible in the XAS, however, as can be seen from Fig. 4 these transitions slightly reduce the intensity of the low energy peak in the L_3 and L_2 XMCD spectra.

A qualitative explanation of the XMCD spectra shape is provided by the analysis of the corresponding selection rules,

TABLE I. The dipole allowed transitions from core $2p_{1/2,3/2}$ levels to the unoccupied $5d_{3/2,5/2}$ valence states for left ($\lambda=+1$) and right ($\lambda=-1$) polarized x-rays.

Edge	$\lambda=+1$	$\lambda=-1$
L_3	$-3/2 \rightarrow -1/2$	$-3/2 \rightarrow -5/2$
	$-1/2 \rightarrow +1/2$	$-1/2 \rightarrow -3/2$
	$+1/2 \rightarrow +3/2$	$+1/2 \rightarrow -1/2$
	$+3/2 \rightarrow +5/2$	$+3/2 \rightarrow +1/2$
L_2	$-1/2 \rightarrow +1/2$	$-1/2 \rightarrow -3/2$
	$+1/2 \rightarrow +3/2$	$+1/2 \rightarrow -1/2$

orbital character and occupation numbers of individual $5d$ orbitals. Because of the electric dipole selection rules ($\Delta l = \pm 1; \Delta j = 0, \pm 1$) the major contribution to the absorption at the L_2 edge stems from the transitions $2p_{1/2} \rightarrow 5d_{3/2}$ and that at the L_3 edge originates primarily from $2p_{3/2} \rightarrow 5d_{5/2}$ transitions, with a weaker contribution from $2p_{3/2} \rightarrow 5d_{3/2}$ transitions. For the latter case the corresponding $2p_{3/2} \rightarrow 5d_{3/2}$ radial matrix elements are only slightly smaller than for the $2p_{3/2} \rightarrow 5d_{5/2}$ transitions. The angular matrix elements, however, strongly suppress the $2p_{3/2} \rightarrow 5d_{3/2}$ contribution. Therefore the contribution to XMCD spectrum at the L_3 edge from the transitions with $\Delta j=0$ is one order of magnitude smaller than the transitions with $\Delta j=1$.[8]

The selection rules for the magnetic quantum number m_j (m_j is restricted to $-j, \ldots, +j$) are $\Delta m_j=+1$ for $\lambda=+1$ and $\Delta m_j=-1$ for $\lambda=-1$. Table I presents the dipole allowed transitions for x-ray absorption spectra at the L_3 and L_2 edges for left ($\lambda=+1$) and right ($\lambda=-1$) polarized x rays.

To go further, we need to discuss the character of the $3d$ empty DOS. Since l and s prefer to couple antiparallel for less than half-filled shells, the $j=l-s=3/2$ has a lower energy than the $j=l+s=5/2$ level. Due to the intra-atomic exchange interaction the lowest sublevel of the $j=3/2$ will be $m_{3/2}=-3/2$, however, for the $j=5/2$ the lowest sublevel will be $m_{5/2}=+5/2$. This reversal in the energy sequence arises from the gain in energy due to alignment of the spin with the exchange field.

The contribution to the L_3 absorption spectrum from the first two transitions (Table I) for $\lambda=+1$ cancels to a large extent with the contribution of opposite sign from the last two transitions for $\lambda=-1$ having the same final states. Thus the XMCD spectrum of Gd at the L_3 edge ($I=\mu^- - \mu^+$) can be approximated by the following sum of m_j–projected partial densities of states $(N^{5/2}_{-5/2}+N^{5/2}_{-3/2})-(N^{5/2}_{3/2}+N^{5/2}_{5/2})$. Here we use the notation $N^j_{m_j}$ for the density of states with the total momentum j and its projection m_j. From this expression one would expect the L_3 XMCD spectrum with two peaks of opposite signs with almost the same intensity. The corresponding L_2 XMCD spectrum can be approximated by the following partial DOS's: $(N^{3/2}_{-1/2}+N^{3/2}_{-3/2})-(N^{3/2}_{1/2}+N^{3/2}_{3/2})$. From this expression one would also expect two peak structure of L_2 XMCD spectrum with an opposite signs. In addition, due to the reversal energy sequences for the $j=3/2$ and $j=5/2$ sublevels the energy positions of the positive and negative

peaks are opposite to each other for the L_3 and L_2 XMCD spectra.

We should note, however, that the explanation of the XMCD line shape in terms of m_j-projected DOS's presented above should be considered as only qualitative. First, there is no full compensation between transitions with equal final states due to difference in the angular matrix elements; second, in our consideration we neglect cross terms in the transition matrix elements. In addition, we have used the *jj*-coupling scheme here, however, the combination of the hybridization, Coulomb, exchange and crystal-field energies may be so large relative to the 5*d* spin-orbit energy that the *jj* coupling is no longer an adequate approximation.

The XMCD spectra at the Gd $L_{2,3}$ edges are mostly determined by the strength of the spin-orbit (SO) coupling of the initial Gd 2*p* core states and spin polarization of the final empty $5d_{3/2,5/2}$ states while the exchange splitting of the Gd 2*p* core states as well as the SO coupling of the 5*d* valence states are of minor importance for the XMCD at the Gd $L_{2,3}$ edges of GdN.

Recently Leuenberger *et al.*[22] measured XAS and XMCD spectra at the Gd $L_{2,3}$ edges in thin films of the GdN with a lattice constant 4.4% above that of bulklike layers (which corresponds to increasing the unit-cell volume at 8.6%). The nonequilibrium structure is obtained by N^+ plasma-assisted reactive sputter deposition at room temperature. The Curie temperature T_C was found to be significantly diminished in the nonequilibrium situation: it lies near 30 K for GdN deposited at room temperature as compared to the bulk value of 60 K found for the layers deposited at T_S=450°. It was found that an enhancement of the lattice parameter does not lead to a significant change in the $L_{2,3}$ x-ray absorption and dichroism at the L_3 edge. However, the XMCD spectrum at the L_2 edge became wider and reduced in intensity. It leads to significant deviation of the ratio of the XMCD amplitudes, L_3/L_2, which has a value of almost 3 up to 100 K and then decreases slightly toward higher temperature. These values are far above the observed for Gd based systems,[41] and the value found for the bulklike GdN layer. One should mention that Gd $L_{2,3}$ XA spectra in GdN for the bulk and the expanded lattices were acquired by means of different spectrometers and different methods.[22] The lattice expanded GdN layers were measured at the energy-dispersive beamline D11 of the DCI storage ring at the French synchrotron facility LURE in Orsay in transmission mode, however, the bulklike layers were recorded at the beamline ID12A of the European Synchrotron Radiation Facility in Grenoble, France using the total fluorescence-yield (TFY) method.

We carried out the LSDA+*U* band structure and XMCD calculations for the expanded lattice constant of 5 and 10 % above the bulklike one. If the energy band structure for the bulk GdN corresponds to the half-metallic solution with the energy gap only in the minority channel, the band structure for the expanded lattice constants became a semiconductor type with an indirect gap between Γ and *X* symmetry points equal to 0.008 and 0.17 eV for the 5 and 10 % expansion, respectively. The increasing of the lattice constant leads to the decreasing of Gd empty $5d_{3/2,5/2}$ width, besides the corresponding DOS's are shifted towards the Fermi level. The occupied number is slightly decrease, however the *d* spin and orbital moments are changed insignificantly with increasing of the lattice constant. The XMCD spectra at the $L_{2,3}$ edges slightly increase their intensity for the expanded lattice without any significant changing in the shape. The Gd XMCD L_3/L_2 ratio also does not changed. Therefore a strong increase of the XMCD ratio L_3/L_2 with the expanded lattice volume observed in the GdN layers in Ref. 22 could not be explained by simple expansion of the lattice constant.

We also studied the SO coupling by scaling the corresponding terms in the Hamiltonian artificially with a constant prefactor in the framework of the LSDA+*U* method. The scaling of the SO coupling at the Gd site by a factor of 2, 3, and 4 leads to decreasing of the L_2 XMCD amplitude by 1.3, 1.5, and 2.3 times, respectively. However, the L_3 XMCD spectrum almost does not change its intensity. For the largest scaling factor used, the Gd 5*d* orbital moment is increased by 1.8 times, however, the most dramatic changing occurs for the Gd 4*f* orbital moment. It increased from the value of $0.063\mu_B$ for the ground state up to 0.280, 0.704, and $1.387\mu_B$ for the scaling factor equal to 2, 3, and 4, respectively.

It is hard to believe that for some reason the SO interaction can increase so much. However, the Gd orbital magnetism can be significantly changed when we go beyond a half filled $4f^7$ shell, considering the possible existence of the Gd^{2+} ($4f^8$) or the Gd^{4+} ($4f^6$) ions in some nonequilibrium conditions. Using a supercell approximation with four formula units we were able to obtained a self-consistent solution with one of four Gd ions in the $4f^6$ state due to the $4f \rightarrow 5d$ promotion effect. Technically speaking it is still a Gd^{3+} ion but instead of the $4f^7$ configuration we have the $4f^65d^1$ one. The solution provides the $j=7/2$, $m_j=-7/2$ for the created 4*f* hole which gives the Gd orbital magnetic moment equal to $-2.756\mu_B$. This is twice as much as the results obtained with the artificial SO scaling factor of four. The 5*d* orbital magnetic moment also became three times larger in comparison with ground state with the $4f^7$ configuration. The $L_{2,3}$ XA spectra for the $4f^65d^1$ Gd are shifted towards lower energy in comparison with the $4f^7$ Gd spectra. As a result XMCD spectra obtained as a sum of spectra from the $4f^65d^1$ and the $4f^7$ Gd ions became wider and reduce their intensity. We have been able even to reproduce the shape of the experimental L_2 XMCD spectrum in the GdN observed in the expanded lattice, however, the ratio of the XMCD amplitudes L_3/L_2 still changed insignificantly.

We should also mentioned that the total energy for the solution with one of four Gd ions in the $4f^65d^1$ state is significantly higher (2.8 eV/f.u.), than with all four ions in the $4f^7$ state. It might be interesting to measure the XMCD $L_{2,3}$ spectra in some rare-earth compounds, for example, some samarium or europium chalcogenides or pnictides with different valencies. The magnetism of the Eu^{2+} (configuration $4f^7$) and Eu^{3+} (configuration $4f^6$) ions is the reverse of that of the Sm^{2+} ($4f^6$) and Sm^{3+} ($4f^5$) ions, i.e., the trivalent Eu ion has the same magnetic ground state of $J=0$ as that of the divalent Sm ion. The magnetic ground state of the Eu^{2+} ions is $J=7/2$ with no orbital moment.[42]

We should mention that the electronic and magnetic structures of GdN are very sensitive to the quality of the sample. Actually the lack of sufficient reliable experimental information on the fundamental properties of GdN is related to the

problem of sample preparation.[3] The high melting point makes it very difficult to grow crystals with good stoichiometry and well-defined properties. The early discrepancies concerning the magnetic ground-state configuration: ferromagnetic[43,44] or antiferromagnetic,[1,45] for example, may be related to a different degree of sample perfection. One can imagine that the expanded lattice in low T sputtered GdN might contain some an additional interstitial N atoms. That would totally change the symmetry, introducing a $L=1$ component to the crystal field (CF) (cubic systems allows only $L=0, 4, 6, \ldots$, crystal field splitting) and allow $L=3$ and $L=2$ direct coupling $\langle 4f|V_{\mathrm{CF}}|5d\rangle$, which might significantly change the $4f$–$5d$ hybridization and the L_3/L_2 XMCD amplitudes. As an indirect evidence for such a possibility we can point out that the unusual relation between the dichroic L_2 and L_3 edge signals was observed previously upon hydrogen charging of R-based multilayers.[46] This interesting question needs additional experimental and theoretical investigations.

D. N *K* XMCD spectrum

The XA and XMCD spectra in metals at the K edge in which the $1s$ core electrons are excited to the p states through the dipolar transition usually attract only minor interest because p states are not the states of influencing magnetic or orbital order. Recently, however, understanding p states has become important since XMCD spectroscopy using K edges of transition metals became popular. The K edge XMCD is sensitive to electronic structures at neighboring sites, because of the delocalized nature of the p states.

It is documented that sizable XMCD signals can be detected at the K edge of nonmagnetic atoms, such as sulfur and oxygen in ferromagnetic EuS (Ref. 47) EuO,[48] respectively. The experimental K edge photoabsorption and XMCD spectra of nitrogen in GdN were investigated by Leuenberger *et al.*[21] It was found that the dichroic peak amplitude amounts to 4% of the edge jump of the isotropic XA spectrum at 401 eV (Fig. 5), which is a remarkably large value for K edge XMCD. The N K edge dichroic signal in GdN is about three times larger than at the K edge of oxygen in EuO and exceeds that at the K edge of sulfur in EuS by an order of magnitude; it surpasses even that at the onsite Fe K edge of iron metal where it is on the order of 0.3%.[49]

A comparison of the XMCD spectra with the theoretical partial density of empty N p states calculated by Aerts *et al.*[15] shows considerable disparities that were not well understood.[21] Clearly, to reproduce the XMCD spectra one has to include the transition matrix elements.

Figure 5 shows the theoretically calculated x-ray absorption spectra at the N K edge as well as XMCD spectra in GdN in comparison with the corresponding experimental data.[21] The experimentally measured XA spectrum has a three peak structure. The first maximum in the spectrum is at around 400 eV which has a low energy shoulder not reproduced in the theoretical LSDA or LSDA+U calculations. The energy position of the theoretical second peak at around 402 eV is in good agreement with the experimental measurements. The position of the third high energy peak is shifted to higher energy in the theory.

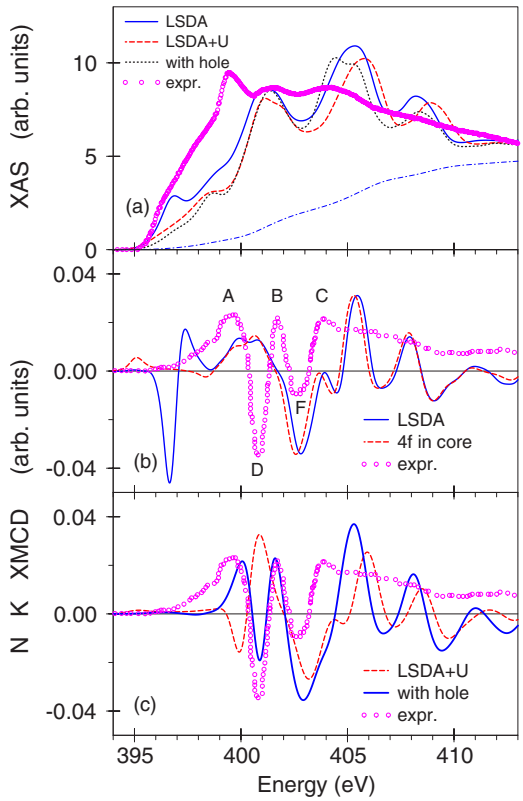

FIG. 5. (Color online) (a) The experimental (Ref. 21) (circles) isotropic absorption spectrum of GdN at the N K edge in comparison with the calculated ones using the LSDA (full line) and LSDA+U approximations without (dashed line) and with (dotted line) taking into account the core-hole effect. Experimental spectra were measured with external magnetic field (0.1 T) at 15 K. Dashed-dotted line shows the theoretically calculated background spectrum (b) experimental (Ref. 21) (circles) XMCD spectrum of GdN at the Gd K edge in comparison with theoretically calculated ones using the LSDA (full line) and putting the $4f$ states in core (dashed line) approximations; (c) experimental (circles) XMCD Gd K spectrum in comparison with theoretically calculated using the LSDA+U approximation with (full line) and without (dashed line) taking into account the core-hole effect.

Figure 5(b) shows the experimental XMCD spectrum[21] and theoretically calculated ones using the LSDA approximation and with $4f$ electrons placed in the core. The experimental spectrum is very complicated and consists of three positive (A, B, C) and two negative (D, F) peaks. The LSDA calculations as well the calculations with $4f$ electrons in the core give a completely inadequate description of the shape of N K XMCD spectrum. The most prominent discrepancy in the LSDA XMCD spectrum is the resonance structure with negative and positive peaks at around 396 to 398 eV which is caused by the strong hybridization of unoccupied Gd N p states with the $4f$ states situated too close to the Fermi level in the LSDA calculations. This structure disappears when we put $4f$ electrons in core.

The N $2p$–Gd $(4f,5d)$ hybridization and the spin-orbit interaction in the $2p$ states play crucial roles for the N K edge dichroism. The K XMCD spectra come from the orbital polarization in the empty p states, which may be induced by

(1) the spin polarization in the p states through the spin-orbit interaction and (2) the orbital polarization at neighboring sites through hybridization. We calculated the K XMCD spectrum at N site with turning the SOI off separately on the N $2p$ states and at the Gd site (at both the $4f$ and $5d$ states), respectively. We found that the K XMCD spectrum is slightly changed when the SOI on the N site is turned off, while the spectrum almost disappears (reduced its intensity almost two order of magnitude) when the SOI on the Gd site is turned off. This indicates that the SOI on Gd site is influencing the orbital mixture of N $2p$ states through the N $(2p)$–Gd (d,f) hybridization.

The effect of SOI and exchange splitting on the magneto-optical and XMCD spectra of solids has been studied by several authors.[50–56] The LSDA+U approach [Fig. 5(c)] improves the agreement between theory and the experiment, especially in describing the peak B. However, LSDA+U theory fails to produce the peak A, in addition to the peaks B and D are shifted towards lower energy at around 0.6 eV in comparison with the experimental measurements. Also for the energies higher than peak C theory gives some additional oscillating structures, while the experimental spectrum is a smooth positive function of energy.

We investigate also the core-hole effect in the final state using the supercell approximation. In our calculations we used a supercell containing eight conventional GdN cells. At one of the eight N atoms we create a hole at the $1s$ level for the self-consistent LSDA+U calculations of the K spectrum. We found that the core-hole interactions significantly improve the agreement between theoretically calculated and experimentally measured N K XMCD spectra [Fig. 5(c)]. The oscillation behavior of the high energy part of the theoretical spectrum above 405 eV could possibly be damped by the quasiparticle lifetime effect, which is not taken into account in our calculations. The core-hole effect improves also the agreement in the energy position of the third high energy peak in the XAS [Fig. 5(a)].

However, all the calculations were not able to produce the first maximum of the N K XAS above the edge at around 400 eV. One of the possible reasons for such disagreements might be the surface effect. The N K edge occurs at a relatively small energy and one would expect larger surface affects at the N K edge than, for example, at the Gd $M_{4,5}$ or $L_{2,3}$ edges. To model the surface effects we carried out band structure calculations using a tetragonal supercell containing four unit cells of GdN along the z direction in which three GdN layers are replaced by three layers of empty spheres. We calculated the XAS and XMCD spectra at N K edge for such a five layer slab separated by three layers of empty spheres [5/3 multilayered structure (MLS)] using the LSDA+U approximation. We also carried out the band structure calculations for a nine layer slab separated by three layers of empty spheres (9/3 MLS). We found that the K XMCD spectrum for N in the middle of the 9/3 MLS (fifth layer) is identical to the corresponding bulk LSDA+U spectrum (not shown). The corresponding spectrum for the middle layer in the 5/3 MLS (third layer) is still slightly different from the bulk spectrum, therefore the convergence was achieved only in the 9/3 MLS. Figure 6 shows the N p empty partial DOS's for the surface layer in the 9/3 MLS and the bulk structure in comparison with the experimental XA spectrum at the N K edge. It can be seen that the partial DOS strongly increases at the first maximum above the edge for the surface layer.

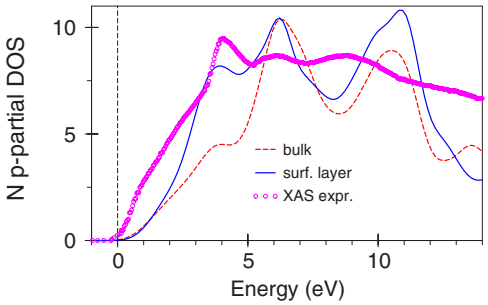

FIG. 6. (Color online) N p empty partial DOS's (in arbitrary units) for the surface layer in the 9/3 MLS (full line) and the bulk structure (dashed line) in comparison with the experimental XA spectrum at the N K edge (Ref. 21) (circles).

Actually the importance of the surface effect has some experimental evidence. The authors of Ref. 21 mention that the spectral feature at 400 eV was not contained in a preliminary N K edge XA spectrum recorded on a Cr-covered 30 Å GdN layer using the total fluorescence yield detection mode due to the larger probing depth of this method compared to the measurements with the total electron yield (TEY) detection in Ref. 21. This indicates that the first maximum above the edge in the XA spectrum at 400 eV is likely related to the GdN surface or interface where the TEY detection is sensitive. The peak is a signature of the surface GdN XA behavior of the sample. This also applies for the slowly rising part of the XMCD signal below 400 eV. This result supports our conclusion that the first maximum above the edge in the XA spectrum might be related to the GdN surface or interface.

It is also important to note that the energy position of the first XA maximum above the edge at around 400 eV coincides with the position of the Gd $4f$ DOS and any kind of change in the N $2p$–Gd $4f$ hybridization (which we discussed in previous paragraph) might influence the intensity of the XAS at that energy. The possible existence of interstitial N atoms may also influence the low energy part of the spectrum via stronger direct Gd $4f$–N $2p$ hybridization.

IV. SUMMARY

GdN is a system with a strongly correlated electronic structure and a low concentration of free charge carriers. We have studied the electronic structure and x-ray magnetic circular dichroism spectra in GdN using the LSDA, LSDA+U approximations, and with $4f$ electrons in core by means of an *ab initio* fully-relativistic spin-polarized Dirac linear muffin-tin orbital method. We found good agreement between calculated and experimental XAS and XMCD spectra at the Gd $L_{2,3}$, $M_{4,5}$, and N K edges.

The theoretically calculated XA spectra at the $M_{4,5}$ edges have a rather simple line shape composed of two white line peaks with additional fine structures at the high energy part of the spectra which can be assigned to multiplet structures. The dichroism at the Gd $M_{4,5}$ edges is very large (it amounts

to more than 20% of the edge jump of the corresponding isotropic XA spectra) due to strong spin orbit coupling of the initial Gd $3d$ core states and large spin polarization of the final empty $4f_{5/2,7/2}$ states.

The LSDA+U calculations show good agreement in the shape of the Gd XA spectra at the $L_{2,3}$ edges with the experimental measurements. They also reproduce the observed two lobe structure of the Gd XMCD spectra for the bulklike layers, however, the theory overestimates the smaller lobe and underestimates the larger one at both the L_3 and L_2 edges. A dramatic increase of the dichroic signal amplitude ratio L_3/L_2, in the GdN lattice-expanded layers observed in Ref. 22 could not be explained by simple expansion of the lattice constant and needs additional theoretical and experimental investigations.

The N $2p$ – Gd $(4f,5d)$ hybridization and the spin-orbit interaction in the $2p$ states play a crucial role for the N K edge dichroism. We found that the N $2p$ orbital polarization originates mainly from the large spin polarization at neighboring Gd atoms through the N $(2p)$–Gd (d,f) hybridization. This mechanism is different from the XMCD in transition metal compounds in which the $4p$ orbital polarization is induced mostly by the $4p$ spin polarization at the atom itself through the SOI.

We investigated the core-hole effect in the final states using a supercell approximation. The final-state interaction improves the agreement between the theory and the experiment at the $M_{4,5}$ and N K edges, however, it has a minor influence on the shape of the Gd $L_{2,3}$ XMCD spectra. We found that the peak at 400 eV in XAS might be related to the GdN surface or interface.

Due to delocalized nature of the p states and wide spread of p wave functions K XMCD spectra are very sensitive to the surrounding neighborhood and, hence, the K XMCD spectroscopy can be used as an effective probe which can detect details of magnetic interatomic interactions in rare-earth compounds.

ACKNOWLEDGMENTS

This work was carried out at the Ames Laboratory, which is operated for the U.S. Department of Energy by Iowa State University under Contract No. W-7405-82. This work was supported by the Office of Basic Energy Sciences of the U.S. Department of Energy. V. N. Antonov gratefully acknowledges the hospitality at the Ames Laboratory during his stay.

[1] P. Wachter and E. Kaldis, Solid State Commun. **34**, 241 (1980).
[2] P. Wachter, in *Handbook of the Physics and Chemistry of Rare Earths*, edited by K. A. Gschneidner, L. Eyring, and S. Hüfner (North-Holland, Amsterdam, 1994), Vol. 19, p. 177.
[3] D. X. Li, Y. Haga, H. Shida, T. Suzuki, Y. S. Kwon, and G. Kido, J. Phys.: Condens. Matter **9**, 10777 (1997).
[4] A. Hasegawa and A. Yanase, J. Phys. Soc. Jpn. **42**, 492 (1977).
[5] A. G. Petukhov, W. R. L. Lambrecht, and B. Segall, Phys. Rev. B **53**, 4324 (1996).
[6] W. R. L. Lambrecht, Phys. Rev. B **62**, 13538 (2000).
[7] S. A. Wolf, D. D. Awschalom, R. A. Buhrman, J. M. Daughton, S. von Molnar, M. L. Roukes, A. Y. Chtchelkanova, and D. M. Treger, Science **294**, 1488 (2001).
[8] V. Antonov, B. Harmon, and A. Yaresko, *Electronic Structure and Magneto-optical Properties of Solids* (Kluwer Academic, Dordrecht, 2004).
[9] J. P. Perdew and A. Zunger, Phys. Rev. B **23**, 5048 (1981).
[10] V. I. Anisimov, J. Zaanen, and O. K. Andersen, Phys. Rev. B **44**, 943 (1991).
[11] L. Hedin, Phys. Rev. **139**, A796 (1965).
[12] W. Metzner and D. Vollhardt, Phys. Rev. Lett. **62**, 324 (1989).
[13] T. Pruschke, M. Jarell, and J. K. Freericks, Adv. Phys. **44**, 187 (1995).
[14] A. Georges, G. Kotliar, W. Krauth, and M. J. Rozenberg, Rev. Mod. Phys. **68**, 13 (1996).
[15] C. M. Aerts, P. Strange, M. Horne, W. M. Temmerman, Z. Szotek, and A. Svane, Phys. Rev. B **69**, 045115 (2004).
[16] C. Duan, R. F. Sabiryanov, J. Liu, W. N. Mei, P. A. Dowben, and J. R. Hardy, Phys. Rev. Lett. **94**, 237201 (2005).
[17] S. Kalvoda, M. Dolg, H. J. Flad, P. Fulde, and H. Stoll, Phys. Rev. B **57**, 2127 (1998).
[18] A. Sharma and W. Nolting, J. Phys.: Condens. Matter **18**, 7337 (2006).
[19] D. B. Ghosh, M. De, and S. K. De, Phys. Rev. B **72**, 045140 (2005).
[20] P. Larson and W. R. L. Lambrecht, Phys. Rev. B **74**, 085108 (2006).
[21] F. Leuenberger, A. Parge, W. Felsch, K. Fauth, and M. Hessler, Phys. Rev. B **72**, 014427 (2005).
[22] F. Leuenberger, A. Parge, W. Felsch, F. Baudelet, C. Giorgetti, E. Dartyge, and F. Wilhelm, Phys. Rev. B **73**, 214430 (2006).
[23] F. Leuenberger, A. Parge, W. Felschb, T. Neisius, and O. Mathon, J. Appl. Phys. **100**, 033905 (2006).
[24] V. N. Antonov, B. N. Harmon, and A. N. Yaresko, Phys. Rev. B **64**, 024402 (2001).
[25] O. K. Andersen, Phys. Rev. B **12**, 3060 (1975).
[26] V. V. Nemoshkalenko and V. N. Antonov, *Computational Methods in Solid State Physics* (Gordon and Breach, Amsterdam, 1998).
[27] J. P. Perdew and Y. Wang, Phys. Rev. B **45**, 13244 (1992).
[28] P. E. Blöchl, O. Jepsen, and O. K. Andersen, Phys. Rev. B **49**, 16223 (1994).
[29] J. C. Fuggle and J. E. Inglesfield, *Unoccupied Electronic States. Topics in Applied Physics* (Springer, New York, 1992), Vol. 69.
[30] F. K. Richtmyer, S. W. Barnes, and E. Ramberg, Phys. Rev. **46**, 843 (1934).
[31] V. N. Antonov, O. Jepsen, A. N. Yaresko, and A. P. Shpak, J. Appl. Phys. **100**, 043711 (2006).
[32] A. N. Yaresko, V. N. Antonov, and P. Fulde, Phys. Rev. B **67**, 155103 (2003).
[33] V. N. Antonov, B. N. Harmon, and A. N. Yaresko, Phys. Rev. B **63**, 205112 (2001).
[34] V. N. Antonov, B. N. Harmon, and A. N. Yaresko, Phys. Rev. B **66**, 165208 (2002).

[35] W. E. Pickett, A. J. Freeman, and D. D. Koelling, Phys. Rev. B **22**, 2695 (1980).
[36] J. Lang, Y. Baer, and P. Cox, J. Phys. F: Met. Phys. **11**, 121 (1981).
[37] Y. Baer and W. D. Schneider, in *Handbook of the Physics and Chemistry of Rare Earths*, edited by K. A. Gschneidner, L. Eyring, and S. Hüfner (North-Holland, Amsterdam, 1987), Vol. 10, p. 1.
[38] B. T. Thole, G. van der Laan, J. C. Fuggle, G. A. Sawatzky, R. C. Karnatak, and J.-M. Esteva, Phys. Rev. B **32**, 5107 (1985).
[39] C. Brouder, M. Alouani, and K. H. Bennemann, Phys. Rev. B **54**, 7334 (1996).
[40] J. Schwitalla and H. Ebert, Phys. Rev. Lett. **80**, 4586 (1998).
[41] F. Baudelet, C. Giorgetti, S. Pizzini, C. Brouder, E. Dartyge, A. Fontaine, J. P. Kappler, and G. Krill, J. Electron Spectrosc. Relat. Phenom. **62**, 153 (1993).
[42] V. N. Antonov, B. N. Harmon, and A. N. Yaresko, Phys. Rev. B **72**, 085119 (2005).
[43] G. Busch, J. Appl. Phys. **38**, 1386 (1967).
[44] H. A. A. R. J. Gambino, T. R. McGuire, and S. J. Pickart, J. Appl. Phys. **41**, 933 (1970).
[45] R. A. Cutler and A. W. Lawson, J. Appl. Phys. **46**, 2739 (1975).
[46] M. Münzenberg, F. Leuenberger, W. Felsch, G. Krill, T. Neisius, S. Pascarelli, and S. Pizzini, Phys. Rev. B **67**, 224431 (2003).
[47] A. Rogalev, J. Goulon, and C. Brouder, J. Phys.: Condens. Matter **11**, 1115 (1999).
[48] P. G. Steeneken, Ph.D. thesis, University of Groningen, Groningen, 2002.
[49] G. Schütz, W. Wagner, W. Wilhelm, P. Kienle, R. Zeller, R. Frahm, and G. Materlik, Phys. Rev. Lett. **58**, 737 (1987).
[50] J. I. Igarashi and K. Hirai, Phys. Rev. B **50**, 17820 (1994).
[51] P. M. Oppeneer, V. N. Antonov, T. Kraft, H. Eschrig, A. N. Yaresko, and A. Y. Perlov, J. Appl. Phys. **80**, 1099 (1996).
[52] P. M. Oppeneer, V. N. Antonov, T. Kraft, H. Eschrig, A. N. Yaresko, and A. Y. Perlov, J. Phys.: Condens. Matter **8**, 5769 (1996).
[53] S. Uba, L. Uba, A. Y. Perlov, A. N. Yaresko, V. N. Antonov, and R. Gontarz, J. Phys.: Condens. Matter **9**, 447 (1997).
[54] S. Uba, L. Uba, A. N. Yaresko, A. Y. Perlov, V. N. Antonov, and R. Gontarz, J. Phys.: Condens. Matter **10**, 3769 (1998).
[55] M. Takahashi and J. I. Igarashi, Phys. Rev. B **67**, 245104 (2003).
[56] M. Usuda, J. I. Igarashi, and A. Kodama, Phys. Rev. B **69**, 224402 (2004).